

Geophysical Research Letters

RESEARCH LETTER

10.1029/2019GL082344

Key Points:

- The spring freshet increases the halosteric height in eastern Hudson Bay, generating a seasonal flow
- This anticyclonic seasonal flow pattern is present in observations and the ocean model simulation
- Geostrophic flow that is reinforced by atmospheric forcing drives this springtime flow pattern

Supporting Information:

- Supporting Information S1

Correspondence to:

N. A. Ridenour,
ridenour@ualberta.ca

Citation:

Ridenour, N. A., Hu, X., Sydor, K., Myers, P. G., & Barber, D. G. (2019). Revisiting the circulation of Hudson Bay: Evidence for a seasonal pattern. *Geophysical Research Letters*, 46, 3891–3899. <https://doi.org/10.1029/2019GL082344>

Received 27 SEP 2018

Accepted 14 MAR 2019

Accepted article online 18 MAR 2019

Published online 8 APR 2019

Revisiting the Circulation of Hudson Bay: Evidence for a Seasonal Pattern

Natasha A. Ridenour¹ , Xianmin Hu¹ , Kevin Sydor², Paul G. Myers¹ , and David G. Barber³

¹Department of Earth and Atmospheric Sciences, University of Alberta, Edmonton, Alberta, Canada, ²Manitoba Hydro, Winnipeg, Manitoba, Canada, ³Center for Earth Observation Science, University of Manitoba, Winnipeg, Manitoba, Canada

Abstract The Hudson Bay Complex is the outlet for many Canadian rivers, receiving roughly 900 km³/year of river runoff. Historically, studies found a consistent cyclonic flow year-round in Hudson Bay, due to the geostrophic boundary current induced by river discharge and cyclonic wind forcing that was supported by available observations at that time. Using a high-resolution ocean general circulation model, we show that in summer, the mean circulation is not cyclonic but consists of multiple small cyclonic and anticyclonic features, with the mean flow directed through the center of the bay. Absolute Dynamic Topography and velocity observations also show this seasonal flow pattern. We find that this summer circulation is driven by geostrophic currents, generated by steric height gradients, which are induced by increased river discharge during the spring freshet, and reinforced by anticyclonic seasonal wind patterns.

Plain Language Summary Knowing the direction of the currents, as well as speed, in Hudson Bay is important for understanding regional ocean flow patterns. Currents in Hudson Bay were historically thought to flow counterclockwise. We use a state-of-the-art computer simulation to see if this flow pattern changes during the year. We found that in May and June, the flow pattern in eastern Hudson Bay reverses and the currents flow in a clockwise direction, while currents in western Hudson Bay still flow counterclockwise. Satellite measurements of ocean currents also show this switch in the current direction in eastern Hudson Bay. This reversal of the current direction occurs because of a change in the wind direction as well as the amount of river water entering the bay during spring (May–June). In spring, river water flowing into the bay increases because of snow melt. More river water enters southeastern Hudson Bay, in and around James Bay, causing higher sea levels in the east compared to the west. This water will flow from high to low (east to west), causing the clockwise flow pattern in summer.

1. Introduction

The Hudson Bay Complex (Figure 1) receives about 900 km³/year of river discharge, roughly equal to 25% of what enters the Arctic Ocean (Shiklomanov & Shiklomanov, 2003). Hudson Bay is a shallow, inland sea, with two main sources of freshwater: sea ice melt and river discharge, which have maximum freshwater input during spring and summer, the time of both the spring freshet and sea ice melt (Prinsenberg, 1988). The river discharge induces a geostrophic boundary current, historically believed to generate year-round cyclonic flow in Hudson Bay.

Hudson Bay experiences a full sea ice cycle, being completely ice covered from December–May, as discovered in the late 1940s (Hare & Montgomery, 1949), and ice free from July–September. The spatial distribution of sea ice in Hudson Bay is associated with regional to large-scale atmospheric patterns (Wang et al., 1994a), as well as basin-scale ocean forcing. Ocean currents lead to ice export out of Hudson Bay to Hudson Strait between Southampton Island and Quebec, while wind forcing is responsible for the accumulation of sea ice along the southern and eastern coasts in summer (Wang et al., 1994b).

As Hudson Bay receives a significant amount of discharge, it is possible to use chemical tracers to determine the distribution and pathways of riverine water in the bay. Both Granskog et al. (2007) and Granskog et al. (2009) found evidence of riverine water in the interior of the bay, while the highest concentrations of discharge remained along the coast, agreeing with spatial salinity distributions presented by Ingram

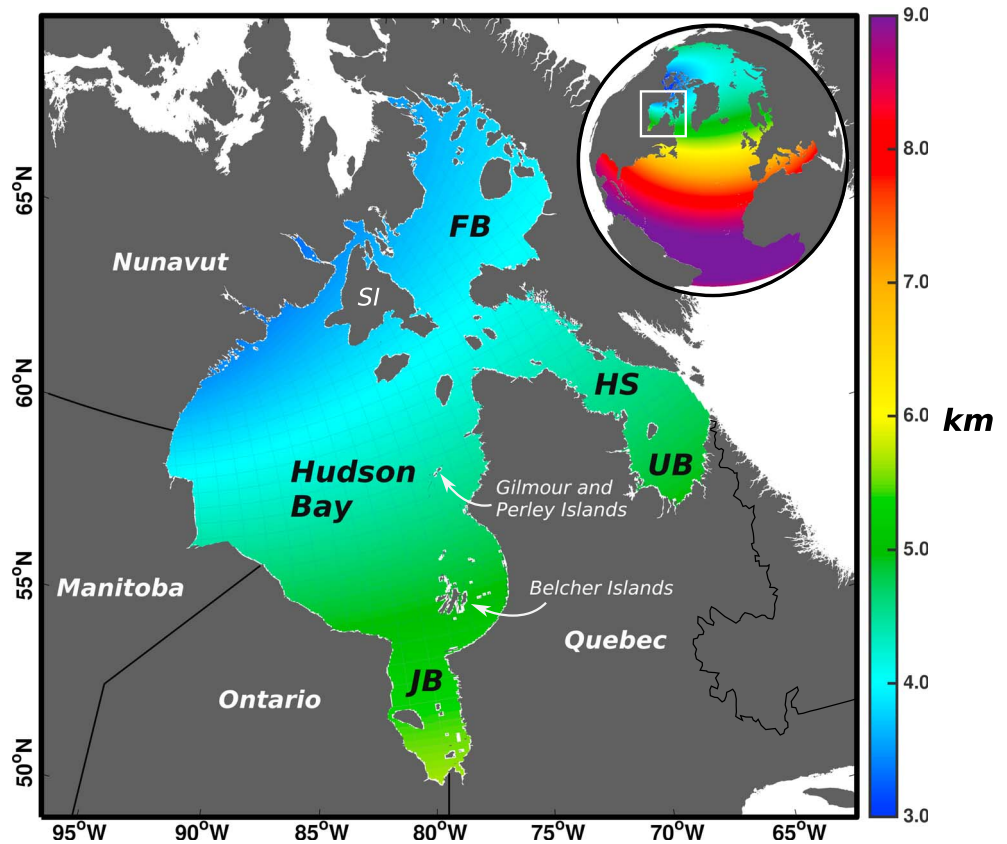


Figure 1. Configuration horizontal resolution (colors, in kilometers) in the Hudson Bay Complex. Thin gray lines show every 15th mesh grid. The ANHA12 configuration horizontal resolution and model domain is shown in the inset. FB denotes Foxe Basin, HS is Hudson Strait, UB for Ungava Bay, and JB for James Bay. Southampton Island is shown by SI. Several additional geographic features are indicated.

and Prinsenber (1998). Extending this analysis, Granskog et al. (2011) found high fractions of river discharge (>5%) in surface waters in the interior and along the coast. Eastern Hudson Bay was also shown to have higher concentrations of riverine water in the water column compared to the west, corresponding to the thickest freshwater layer in James Bay and southeastern Hudson Bay, which decreases northward (Prinsenber, 1984) and westward (Granskog et al., 2011). The interior of Hudson Bay receives freshwater from the boundary via Ekman transport in summer, and in fall, the interior releases this freshwater to the boundary (St-Laurent et al., 2011). In summer, the mean atmospheric forcing is weakly anticyclonic and reverses to strongly cyclonic in fall. St-Laurent et al. (2011) estimated about 25% of riverine water enters the interior, due to the reversal of the winds in summer.

The annual mean circulation in Hudson Bay is stably cyclonic, as determined by observational drift studies conducted as early as the 1930s (Dunbar, 1982; Hachey, 1935; Ingram & Larouche, 1987; Prinsenber, 1986). These results were further supported by modeling studies. Summer circulation was modeled by Wang et al. (1994c), who found stable cyclonic circulation in August (using boundary conditions that constrained the circulation to cyclonic flow), supporting earlier work. While Murty and Yuen (1973) found geostrophic wind stress was an appropriate approximation for simulating cyclonic circulation in September in Hudson Bay, this approximation was not appropriate for the month of May in simulating cyclonic flow. However, Gough et al. (2005) found that the variation in the October–November sea surface height at Churchill is influenced by the May–June discharge in James Bay, explaining 47% of the variability from 1964–1983. The authors concluded that 35–50% of James Bay discharge must flow westward; however, no velocity observations were available to support this statement. Furthermore, evidence of Hudson Strait waters at intermediate depths in northeastern Hudson Bay during summer months suggests that there could be a reversal of the cyclonic boundary current, allowing these waters to enter the bay (Granskog et al., 2011). A comparison of observed and simulated velocities in the northeastern corner of Hudson Bay in St-Laurent et al. (2012) shows a flow

reversal from March to May in current observations at 123-m depth, while a weaker flow reversal is observed at 28-m depth. Higher salinities in the boundary current occurred at the same time as these reversal events. Their model also shows signs of flow reversals in this region.

To our knowledge, there has been no study focusing on the existence of a seasonal flow reversal in Hudson Bay. We use a three-dimensional (3-D) ocean and sea ice coupled model to investigate Hudson Bay circulation in spring and summer, the time of both the spring freshet and ice melt. Satellite and reanalysis data are also used to further support our model results. We find weak anticyclonic circulation in spring and summer in eastern Hudson Bay, which can explain reversals in flow, variability in sea surface height, and the presence of Hudson Strait water at intermediate depths that have been observed in previous studies. The following section describes the model. In section 3, the seasonal circulation in Hudson Bay and its generation are discussed, preceding the discussion.

2. Method

2.1. Numerical Model

In this study, a 3-D, hydrostatic, primitive equation, ocean-sea ice coupled model, based on the Nucleus for European Modelling of the Ocean version 3.4 (Madec & the NEMO team, 2008), is used to carry out the simulations. The ice module is the Louvain-la-neuve Ice Model version 2 with elastic-viscous-plastic rheology (Hunke & Dukowicz, 1997), including both thermodynamic and dynamic processes (Fichefet & Maqueda, 1997). The model configuration used is the Arctic and Northern Hemisphere Atlantic with $1/12^\circ$ resolution (ANHA12; Hu et al., 2018). Within the Hudson Bay Complex, the horizontal resolution is 3.5–5.5 km (Figure 1). In the vertical, there are 50 geopotential levels with the highest resolution (~ 1 m) in the top 10 m. The simulation was integrated from January 2002 to December 2016 with initial fields (3-D temperature, salinity, and horizontal velocities, as well as 2-D sea surface height and sea ice) from GLObal Ocean Reanalysis and Simulations (GLORYS2v3) produced by Mercator Ocean (Masina et al., 2017). At the surface, high spatial (33 km) and temporal (hourly) resolution atmospheric forcing data (10-m wind, 2-m air temperature and specific humidity, downwelling shortwave and longwave radiation flux, and total precipitation) from the Canadian Meteorological Centre's global deterministic prediction system reforecasts described in Smith et al. (2014), are used to drive the model. The GLORYS2v3 data set is also used to provide data (temperature, salinity, and ocean velocities) at the open boundaries, one near Bering Strait, and the other at 20° S in the Atlantic Ocean. Monthly interannual river discharge, corrected by Dai and Trenberth (Dai & Trenberth, 2002; Dai et al., 2009), as well as Greenland melt water provided by Bamber et al. (2012), is also carefully remapped onto the model grid to have more realistic freshwater input from land to ocean. Discharge entering the ocean is prescribed as the same temperature as the surrounding seawater.

Temperature or salinity restoring is not used in the simulation. Thus, freshwater signals will not be damped. Additionally, our configuration does not use tides, as the focus is on large-scale processes. The time step is 180 s, with 5-day averages being used for our analysis. Throughout this paper, spring refers to May–June, which is the time of the spring freshet, and summer is defined as July–September, during the melt season. This was done to separate the effects of freshwater from ice melt and river discharge. Finally, fall is defined as October–December.

2.2. Satellite Observations

To evaluate our model simulation, we use daily mean gridded Absolute Dynamic Topography and geostrophic velocities with $1/4^\circ$ horizontal resolution. These data are altimeter products produced by Ssalto/Duacs and distributed by Aviso, with support from Cnes (<http://www.aviso.altimetry.fr/duacs/>).

2.3. Ocean Reanalysis Data

We also use sea surface height and surface velocity from the Estimating the Circulation and Climate of the Ocean Phase 2 project (Forget et al., 2015; Fukumori et al., 2017), which is an ocean reanalysis product using the Massachusetts Institute of Technology general circulation model. Data, provided in 3-day averages, of these two fields from 2004–2015 are used in this study.

3. Results

Satellite surface geostrophic velocities for summer and fall are shown in Figures 2a and 2b. In summer, these observations show westward flow along the southern coast of Hudson Bay, and northward flow through

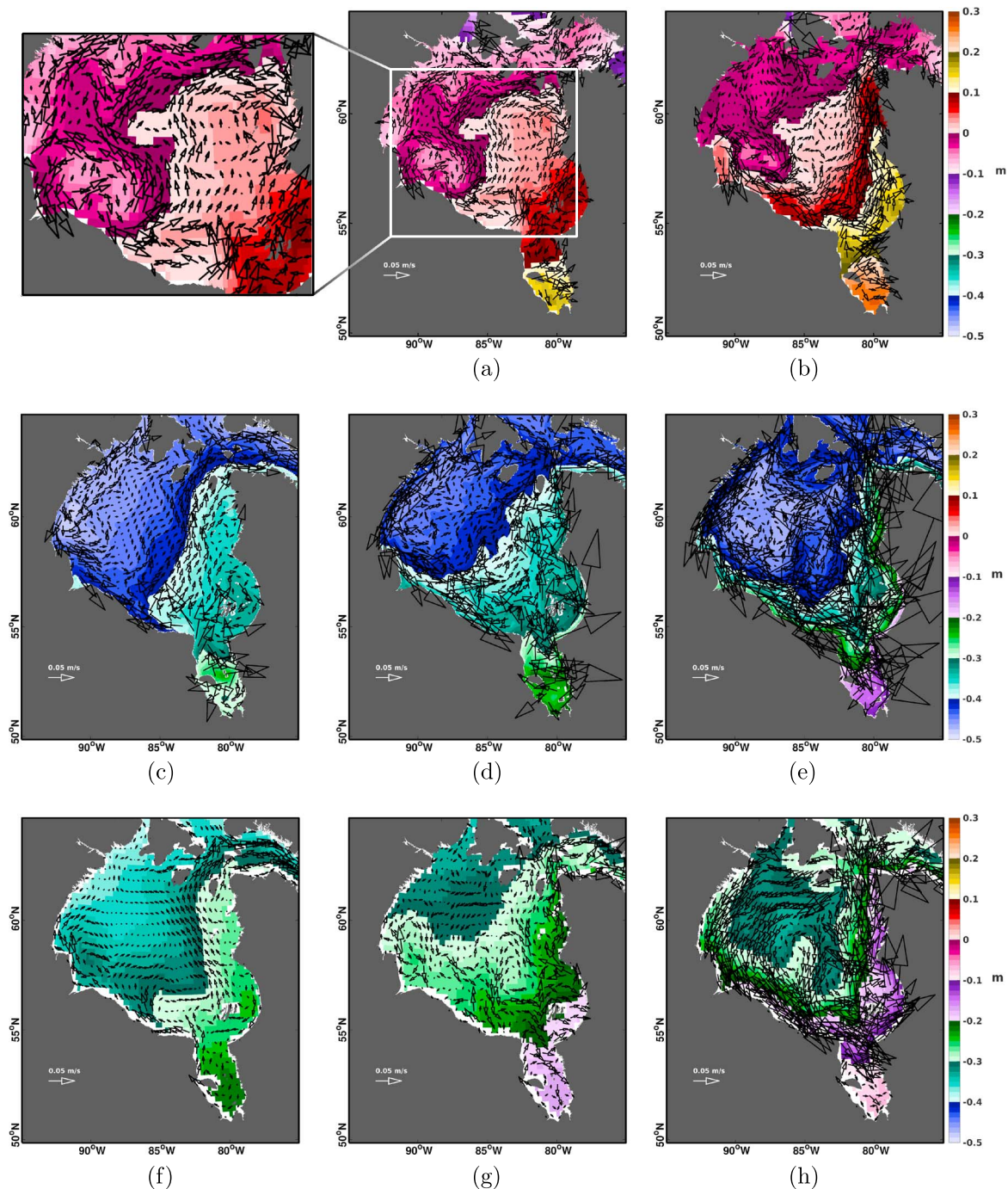


Figure 2. Mean 2004–2015 ocean surface variables shown for Aviso (top), our Arctic and Northern Hemisphere Atlantic with $1/12^\circ$ resolution simulation (middle), and Estimating the Circulation and Climate of the Ocean Phase 2 reanalysis (bottom). Columns from left to right show spring, summer, and fall. The two Aviso panels (a and b) show observed Absolute Dynamic Topography with corresponding surface geostrophic velocities. Absolute Dynamic Topography is the height above the geoid and thus can have positive or negative values. Our model sea surface height and calculated surface geostrophic velocities are shown in panels (c–e). Finally, the three Estimating the Circulation and Climate of the Ocean Phase 2 panels (f–h) show sea surface height with surface velocities. Note the systematic differences between simulations and observations are due to different height references.

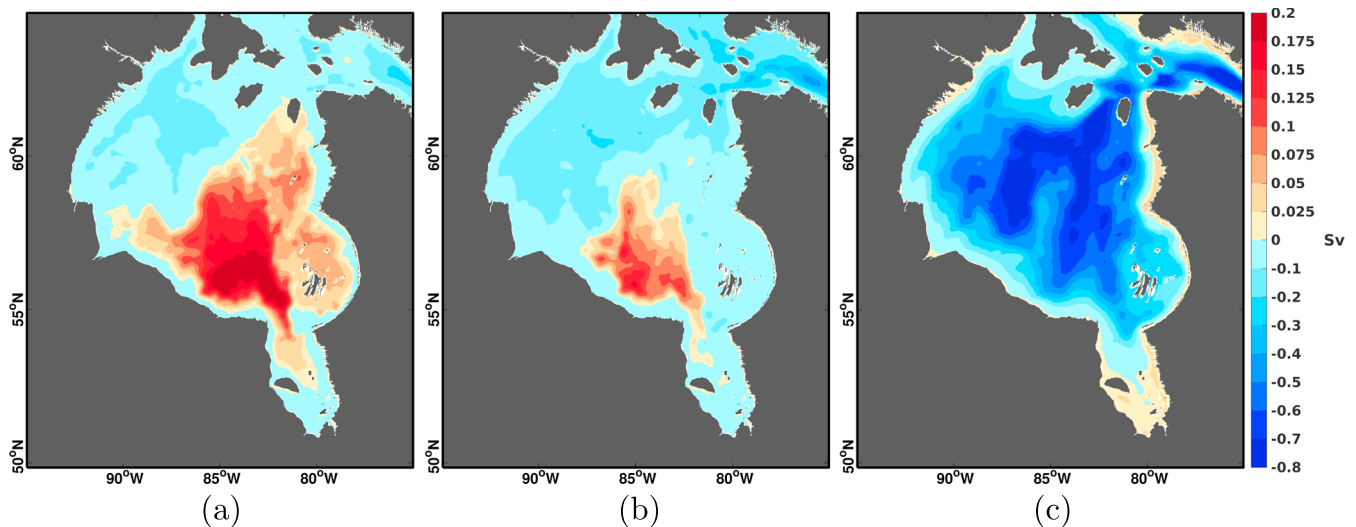


Figure 3. Mean 2004–2015 model barotropic stream function for (a) spring, (b) summer, and (c) fall. The stream function shows velocity vectors as a 2-D scalar value, where the spacing between streamlines provide information on the strength of the flow. Positive (negative) values correspond to anticyclonic (cyclonic) flow.

the center of the bay (Figure 2a). We also see anticyclonic flow around Gilmour and Perley Islands. Northward flow along the western coast and a small cyclonic cell in southwestern Hudson Bay are also seen. In fall we see the strong geostrophic boundary current return to the bay, with weaker flow in the interior (Figure 2b). Satellite altimetry measurements are unreliable in spring due to the presence of sea ice and are therefore not shown. However, model data are not limited to ice free periods; therefore, we show model surface geostrophic velocities for spring, summer, and fall in Figures 2c–2e. Modeled spring and summer geostrophic velocities show flow through the center of the bay. Velocities in our model in fall are larger than those shown in observations; however, our model agrees with the Aviso data, also showing the strong cyclonic boundary current at this time of year.

The bottom panels in Figure 2 show sea surface height and surface velocities from the Estimating the Circulation and Climate of the Ocean Phase 2 reanalysis data set. In spring (Figure 2f), westward flow is present along the southern coast, as well as a meandering flow through the center of the bay. Northward flow is noted along the western coast, while southward flow is seen east of the Belcher Islands. During summer, northward flow is present in northeastern Hudson Bay with a cyclonic recirculation cell near the center of the bay. However, in fall, as with the two other data sets, a very clear cyclonic flow returns to the bay.

A comparison of the sea surface height values from observations and model output in Figure 2 shown in spring (c and f) and summer (a, d, and g) show that gradients decrease gradually from east to west, with a difference of about 10–15 cm across the bay. In fall, however, as the riverine water and sea ice melt are advected northward along the eastern coast, all data sets show larger sea surface height gradients along the eastern coast, driving the strong cyclonic flow.

We calculated the spring, summer, and fall mean model barotropic stream function, shown in Figure 3. The barotropic stream function shows lines of constant volume transport, with units of Sv ($1 \text{ Sv} = 10^6 \text{ m}^3/\text{s}$). The stream function is calculated based on zonal velocity (but with a switch in sign) integrated from south to north. For example, stream function values increasing northward indicate westward flow while stream function values decreasing northward indicate eastward flow. Thus, in Hudson Bay, this corresponds to positive (negative) values for anticyclonic (cyclonic) flow. During spring, we see positive values of the stream function in eastern Hudson Bay, while negative values are in the west (Figure 3a). Note the scale of the positive and negative values. The region with positive values spans over the eastern area but is greatly reduced in summer, during ice melt (Figure 3b). Positive values are lower in magnitude and in area, before disappearing in the fall (Figure 3c), giving way to the cyclonic flow traditionally observed in this region.

To investigate this seasonal flow pattern, and to determine the processes involved, we calculated the spring steric height (Figure 4a) and the seasonal cycle for the curl of both Ekman transport and surface stress (bay-wide average; Figure 4b). Steric height shows the ocean temperature and salinity contributions to changes

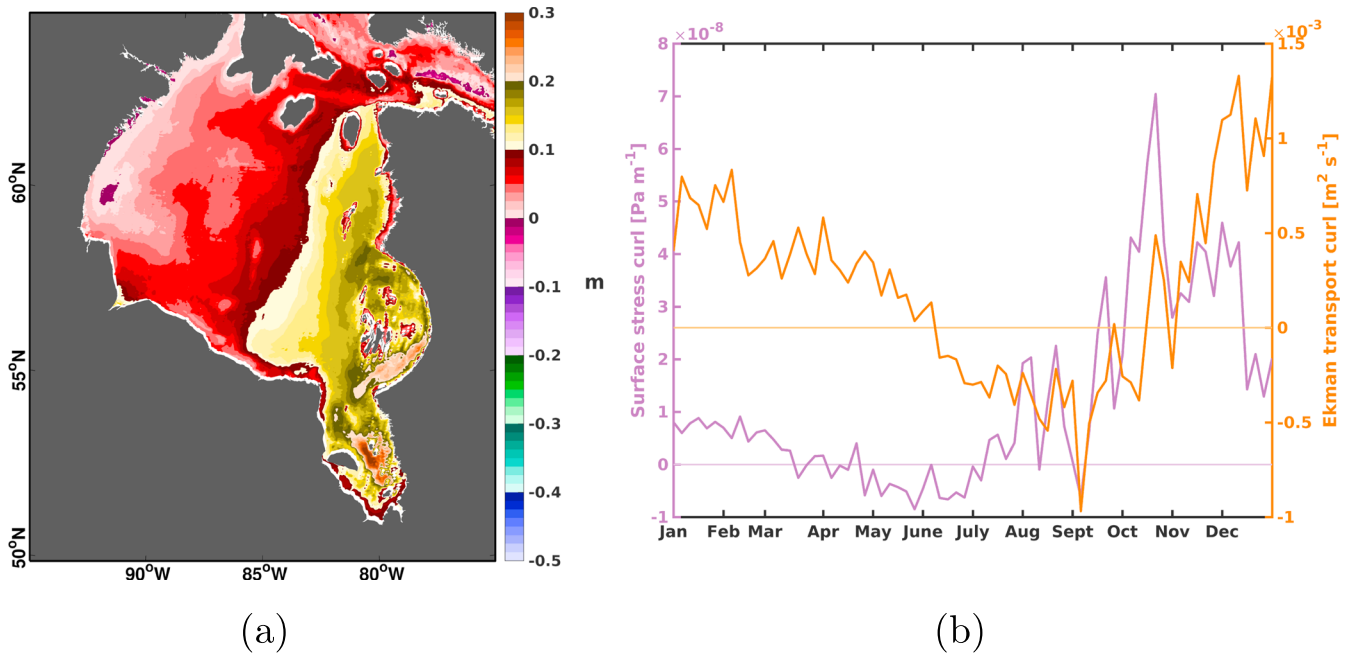


Figure 4. (a) Mean May–June (2004–2015) model halosteric height and (b) seasonal cycles of the surface stress curl (purple) and Ekman transport curl (orange) with zero indicated in each color. Positive (negative) values of the curl indicate cyclonic (anticyclonic) flow.

in sea surface height relative to a reference density. Thus, using this metric, we can determine the role of ocean temperature and salinity in sea surface height variations. We followed Steele and Ermold (2007), where steric height is defined as

$$SH = SH_T + SH_S, \quad (1)$$

$$SH_S = \left[\frac{S_{ref}}{\rho_{ref}} \left(\frac{\partial \rho}{\partial S} \right)_{T_{ref}, S} \right] \int_{sfc}^{bot} \frac{S_{ref} - S}{S_{ref}} dz, \quad (2)$$

$$SH_T = \left[\frac{1}{\rho_{ref}^2 c_p} \left(\frac{\partial \rho}{\partial T} \right)_{T, S_{ref}} \right] \int_{sfc}^{bot} \rho_{ref} c_p (T_{ref} - T) dz, \quad (3)$$

where SH is the steric height and SH_T and SH_S are the thermosteric and halosteric heights, respectively. T_{ref} is the reference temperature, which we chose to be -2°C , with S_{ref} being the reference salinity, at 33. The variables S and T are the salinity and temperature of the seawater accordingly. The reference density, ρ_{ref} , is determined by T_{ref} and S_{ref} , and finally, c_p is the heat capacity of water, with a value of $4,218\text{ J}\cdot\text{K}^{-1}\cdot\text{kg}^{-1}$. Values inside the square brackets are vertical averages. Steric heights were integrated from the surface to the ocean floor.

In spring, thermosteric heights are negligible ($<0.02\text{ m}$), as the bay is still ice covered. Thus, it is the change in salinity that contributes most to steric height in eastern Hudson Bay (Figure 4a). Higher steric heights occur in the east and lower steric heights in the west. The spring freshet, followed by high streamflow during the summer months, lowers the salinity of the waters in the bay, causing steric heights to increase, with the largest amounts of river discharge entering James Bay and southeastern Hudson Bay. In agreement with the steric height distribution, the sea surface height is also higher in the east versus the west (Figure 2c) with a difference of over 10 cm . The sea surface height gradient between western and eastern Hudson Bay induces a westward flow but is deflected to the right by the Coriolis force, and the resulting geostrophic flow is directed through the center of the bay.

Steric height is not the only process leading to changes in sea surface height; wind patterns also play a role. Consistent wind forcing in one direction can cause an accumulation of seawater along a coastline, increasing the sea surface height. The seasonal cycles of baywide averaged surface stress curl and the Ekman transport curl are seen in Figure 4b. The surface wind stress and Ekman transport curl is positive (negative) when there is cyclonic (anticyclonic) flow. The curl of the surface stress (Figure 4b, purple) is positive from January to

around the end of March. During April, the surface stress curl dips below zero, and from May to June, there is anticyclonic surface stress in Hudson Bay, before returning to strong cyclonic surface stress in the fall. The seasonality of the Ekman transport curl (Figure 4b, orange) shows cyclonic flow in the winter and fall; however, from June to mid October, Ekman transport is anticyclonic. Spatially, Ekman transport in eastern Hudson Bay is directed to the west-southwest in May and June (not shown) and rotates to south-southwest in July to September, indicating that the atmosphere might also have a role in seawater accumulation, and increased sea surface height, in southeastern Hudson Bay.

The direction of the geostrophic flow is in agreement with the mean summertime barotropic stream function in Figure 3, and this pattern is consistent with the transport of freshwater from the boundary to the interior in the summer, as suggested by others (St-Laurent et al., 2011). Export of freshwater in the fall occurs when the sea surface height gradient weakens in the interior, decreasing freshwater import. Freshwater is then exported out of the interior in the north, while the strong cyclonic geostrophic current returns to the boundary (Figure 3). The summer and fall circulation patterns are also reinforced by the mean wind circulation in these seasons.

4. Discussion

In this study we investigated seasonal flow patterns in Hudson Bay during spring and summer. Using both observational data and model output, we show circulation in Hudson Bay is not cyclonic year-round. During summer, observations show a small cyclonic cell in southwestern Hudson Bay, and anticyclonic flow in eastern Hudson Bay. Observations from the 1930s (Hachey, 1935) and the 1970s and 1980s, as summarized in Prinsenberg (1986), have implied yearlong cyclonic circulation in the bay. Annual mean circulation in the bay is cyclonic, due to strong cyclonic flow in fall and winter; however, the weak summer circulation has not been captured.

Our findings help explain why Granskog et al. (2011) found high (>5%) concentrations of riverine water in the eastern interior of the bay, as well as the presence of Hudson Strait water at intermediate depths in northeastern Hudson Bay in summer. We are not the first to suggest a westward flow in southern Hudson Bay; however, we are the first to propose an update to the spring and summer circulation pattern in this region. Gough et al. (2005) suggest an advective mechanism, induced by wind forcing as well as discharge in James Bay and southeastern Hudson Bay, whereby discharge from James Bay goes not only north along the Quebec coast but also to the west, impacting the sea surface height in Churchill in the fall. Interestingly, Figure 9 in Saucier et al. (2004), which shows April–June velocities, also implies weak anticyclonic circulation in southeastern Hudson Bay. These studies support our results, yet neither of these papers presented an update to the cyclonic circulation pattern in the bay. Our study pieces together hints of flow reversals from earlier modeling and observational studies to provide a complete picture of a seasonal circulation pattern in Hudson Bay.

To add further support, we have also investigated the spring/summer circulation in other model simulations with coarser resolution ($1/4^\circ$) and different river discharge forcing (see the supporting information; Andersson et al., 2013; Déry et al., 2016; Gelfan et al., 2017; Lindström et al., 2010). In all experiments we find anticyclonic flow in eastern Hudson Bay, with variation in strength due to the discharge data set used. This indicates that modifications to discharge due to anthropogenic changes (Déry & Wood, 2004; Déry et al., 2005, 2011, 2016; McClelland et al., 2006; Shiklomanov & Shiklomanov, 2003) could have implications on seasonal circulation patterns in this region.

Given our findings, we present schematics of mean fall and spring/summer surface circulation patterns for Hudson Bay in Figure 5 based on both model and satellite altimetry analysis shown here. Water from Foxe Basin enters Hudson Bay through Roes Welcome Sound, while water is exported, on average, from Hudson Bay through Southampton Island and Quebec. In spring and summer the circulation changes substantially from the cyclonic circulation previously thought to dominate the flow. Waters continue to flow southward from Foxe Basin through Roes Welcome Sound; however, a cyclonic cell in southwestern Hudson Bay feeds into two currents flowing northward: one just off of the western Hudson Bay coast and another that flows northeastward toward Hudson Strait, through the center of the bay. On the eastern side of the bay, waters from James Bay follow sea surface height contours, which have a local minima along the southern Hudson Bay coast. Flow near the Belcher Islands is generally northward, while to the west of James Bay, flow is westward before being directed northward. A local maxima of sea surface height surrounds Gilmour and

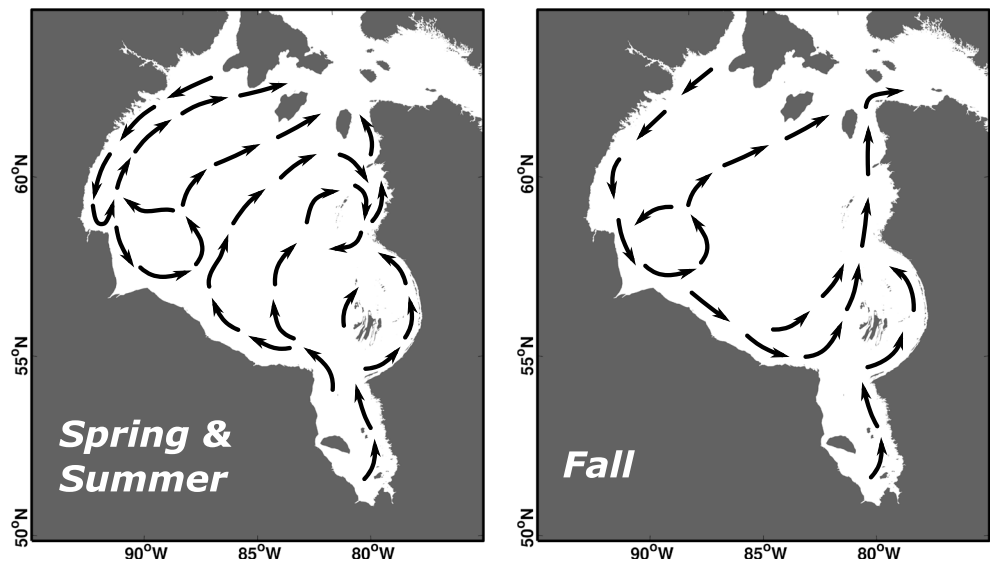


Figure 5. Schematics of average spring/summer and fall surface flow patterns that are based on Aviso satellite altimetry data and model output.

Perley Islands, leading to anticyclonic circulation in northeastern Hudson Bay. This southward flow near the Quebec coast would help explain the current reversals noted by Granskog et al. (2011) and St-Laurent et al. (2012), where Hudson Strait waters enter Hudson Bay. In fall, circulation in the bay is cyclonic, with the strongest flow along the coast. However, observations show a small cyclonic cell in southwestern Hudson Bay and a moderately strong northeastward flow toward Hudson Strait.

This study has shown that during the year, the circulation in Hudson Bay is not consistently cyclonic and that during spring and summer, there is weak anticyclonic flow in eastern Hudson Bay. With this seasonal change in circulation, this raises questions regarding the residence time of river discharge in the bay, and how the bay stores and releases freshwater. Additionally, this updated seasonal circulation may provide insights as to the distribution of nutrients and contaminants around the bay. It also highlights the need for increased observations and observing programs in the bay.

Acknowledgments

CGRF forcing fields are made available by Environment and Climate Change Canada. We thank the Natural Sciences and Engineering Research Council of Canada and Manitoba Hydro for funding the BaySys project (CRDPJ 470028-14), of which this work is part of. This work could not have been possible without the computational resources provided by Westgrid and Compute Canada. Observational data provided by Aviso are greatly appreciated for model evaluation, as well as the use of surface fields from the ECCO2 project. We thank J. Bamber for the use of the Greenland melt data set and Gregory Smith for the use of the CGRF atmospheric forcing. Additionally, we are grateful for the use of GLORYS for initializing our model experiments and forcing the model open boundaries. We appreciate the suggestions provided by two anonymous reviewers, which greatly improved the manuscript.

References

- Andersson, J. C. M., Pechlivanidis, I. G., Gustafsson, D., Donnelly, C., & Arheimer, B. (2013). Key factors for improving large-scale hydrological model performance [Proceedings Paper]. In T. Lekkas (Ed.), *Univ. Aegean, 30, Voulgaroktonou Str, Athens, GR 114 72, Greece* (pp. 77–88): Global Nest, Secretariat. (13th International Conference on Environmental Science and Technology (CEST), Athens, Greece, Sep 05-07, 2013).
- Bamber, J., van den Broeke, M., Ettema, J., Lenaerts, J., & Rignot, E. (2012). Recent large increases in freshwater fluxes from Greenland into the North Atlantic. *Geophysical Research Letters*, *39*, L19501. <https://doi.org/10.1029/2012GL052552>
- Dai, A., Qian, T., Trenberth, K. E., & Milliman, J. D. (2009). Changes in continental freshwater discharge from 1948 to 2004. *Journal of Climate*, *22*(10), 2773–2792. <https://doi.org/10.1175/2008JCLI2592.1>
- Dai, A., & Trenberth, K. E. (2002). Estimates of freshwater discharge from continents: Latitudinal and seasonal variations. *Journal of Hydrometeorology*, *3*(6), 660–687. [https://doi.org/10.1175/1525-7541\(2002\)003h0660:EOFDfC2.0.CO;2](https://doi.org/10.1175/1525-7541(2002)003h0660:EOFDfC2.0.CO;2)
- Déry, S. J., Mlynowski, T. J., Hernández-Henri-quez, M. A., & Straneo, F. (2011). Interannual variability and interdecadal trends in Hudson Bay streamflow. *Journal of Marine Systems*, *88*, 341–351.
- Déry, S. J., Stadnyk, T. A., MacDonald, M. K., & Gauli-Sharma, B. (2016). Recent trends and variability in river discharge across northern Canada. *Hydrology and Earth System Sciences*, *20*(12), 4801–4818.
- Déry, S. J., Stieglitz, M., & McKenna, E. C. (2005). Characteristics and trends of river discharge into Hudson, James, and Ungava Bays, 1964–2000. *Journal of Climate*, *18*(14), 2540–2557.
- Déry, S. J., & Wood, E. F. (2004). Teleconnection between the Arctic Oscillation and Hudson Bay river discharge. *Geophysical Research Letters*, *31*, L18205. <https://doi.org/10.1029/2004GL020729>
- Dunbar, M. (1982). Oceanographic research in Hudson and James Bays. *Le Naturaliste Canadien*, *109*(4), 677–683.
- Fichefet, T., & Maqueda, M. A. M. (1997). Sensitivity of a global sea ice model to the treatment of ice thermodynamics and dynamics. *Journal of Geophysical Research*, *102*(C6), 12,609–12,646. <https://doi.org/10.1029/97JC00480>
- Forget, G., Campin, J.-M., Heimbach, P., Hill, C. N., Ponte, R. M., & Wunsch, C. (2015). ECCO version 4: An integrated framework for non-linear inverse modeling and global ocean state estimation. *Geoscientific Model Development*, *8*(10), 3071–3104. <https://doi.org/10.5194/gmd-8-3071-2015>

- Fukumori, I., Wang, O., Fenty, I., Forget, G., Heimbach, P., & Ponte, R. M. (2017). ECCO version 4 release 3 (*Tech. Rep.*). Pasadena, CA: Jet Propulsion Laboratory, California Institute of Technology. Retrieved from <http://hdl.handle.net/1721.1/110380>, (Available at ftp://ecco.jpl.nasa.gov/Version4/Release3/doc/v4r3_estimation_synopsis.pdf) <https://doi.org/10.1029/2019GL082344>
- Gelfan, A., Gustafsson, D., Motovilov, Y., Arheimer, B., Kalugin, A., Krylenko, I., & Lavrenov, A. (2017). Climate change impact on the water regime of two great Arctic rivers: modeling and uncertainty issues. *Climatic Change*, *141*(3), 499–515. <https://doi.org/10.1007/s10584-016-1710-5>
- Gough, W. A., Robinson, C., & Hosseinian, R. (2005). The influence of James Bay River discharge on Churchill, Manitoba Sea Level. *Polar Geography*, *29*(3), 213–223. <https://doi.org/10.1080/789610202>
- Granskog, M. A., Kuzyk, Z. Z. A., Azetsu-Scott, K., & Macdonald, R. W. (2011). Distributions of runoff, sea-ice melt and brine using $\delta^{18}\text{O}$ and salinity data—A new view on freshwater cycling in Hudson Bay. *Journal of Marine Systems*, *88*, 362–374.
- Granskog, M. A., Macdonald, R. W., Kuzyk, Z. Z. A., Senneville, S., Mundy, C.-J., Barber, D. G., et al. (2009). Coastal conduit in southwestern Hudson Bay (Canada) in summer: Rapid transit of freshwater and significant loss of colored dissolved organic matter. *Journal of Geophysical Research*, *114*, C08012. <https://doi.org/10.1029/2009JC005270>
- Granskog, M. A., Macdonald, R. W., Mundy, C.-J., & Barber, D. G. (2007). Distribution, characteristics and potential impacts of chromophoric dissolved organic matter (CDOM) in Hudson Strait and Hudson Bay, Canada. *Continental Shelf Research*, *27*(15), 2032–2050.
- Hachey, H. B. (1935). Circulation of Hudson Bay water as indicated by drift bottles. *Science*, *82*, 275–276.
- Hare, F. K., & Montgomery, M. R. (1949). Ice, open water, and winter climate in the Eastern Arctic of North America: Part 2. *Arctic*, *2*(3), 149–164.
- Hu, X., Sun, J., Chan, T. O., & Myers, P. G. (2018). Thermodynamic and dynamic ice thickness contributions in the Canadian Arctic Archipelago in NEMO-LIM2 numerical simulations. *The Cryosphere*, *12*(4), 1233–1247. <https://doi.org/10.5194/tc-12-1233-2018>
- Hunke, E. C., & Dukowicz, J. K. (1997). An elastic-viscous-plastic model for sea ice dynamics. *Journal of Physical Oceanography*, *27*(9), 1849–1867. [https://doi.org/10.1175/1520-0485\(1997\)027h1849:AEVPMFi2.0.CO;2](https://doi.org/10.1175/1520-0485(1997)027h1849:AEVPMFi2.0.CO;2)
- Ingram, R. G., & Larouche, P. (1987). Variability of an under-ice river plume in Hudson Bay. *Journal of Geophysical Research*, *92*(C9), 9541–9547. <https://doi.org/10.1029/JC092iC09p09541>
- Ingram, R. G., & Prinsenberg, S. (1998). Coastal oceanography of hudson bay and surrounding eastern canadian arctic waters coastal segment. In A. R. Robinson, & K. H. Brink (Eds.), *The sea* (vol. 11, pp. 835–861). Toronto: John Wiley and Sons.
- Lindström, G., Pers, C., Rosberg, J., Strömqvist, J., & Arheimer, B. (2010). Development and testing of the HYPE (Hydrological Predictions for the Environment) water 394 quality model for different spatial scales. *Hydrology Research*, *41*(3–4), 295–319. <https://doi.org/10.2166/nh.2010.007>
- Madec, G., & the NEMO team (2008). NEMO ocean engine. Note du Pole de Modélisation (No 27 ISSN No 1288–1619).
- Masina, S., Storto, A., Ferry, N., Valdivieso, M., Haines, K., Balmaseda, M., et al. (2017). An ensemble of eddy-permitting global ocean reanalyses from the MyOcean project. *Climate Dynamics*, *49*(3), 813–841. <https://doi.org/10.1007/s00382-015-2728-5>
- McClelland, J. W., Déry, S. J., Peterson, B. J., Holmes, R. M., & Wood, E. F. (2006). A pan-arctic evaluation of changes in river discharge during the latter half of the 20th century. *Geophysical Research Letters*, *33*, L06715. <https://doi.org/10.1029/2006GL025753>
- Murty, T. S., & Yuen, K. B. (1973). Balanced versus geostrophic wind-stress for Hudson Bay. *Journal of the Fisheries Research Board of Canada*, *30*(1), 53–62. <https://doi.org/10.1139/f73-007>
- Prinsenberg, S. J. (1984). Freshwater contents and heat budgets of James Bay and Hudson Bay. *Continental Shelf Research*, *3*(2), 191–200. [https://doi.org/10.1016/0278-4343\(84\)90007-4](https://doi.org/10.1016/0278-4343(84)90007-4)
- Prinsenberg, S. J. (1986). Chapter 10 The circulation pattern and current structure of Hudson Bay. *Elsevier Oceanography Series*, *44*, 187–204. [https://doi.org/10.1016/S0422-9894\(08\)70903-6](https://doi.org/10.1016/S0422-9894(08)70903-6)
- Prinsenberg, S. J. (1988). Ice-cover and ice-ridge contributions to the freshwater contents of Hudson Bay and Foxe Basin. *Arctic*, *41*(1), 6–11. <https://doi.org/10.14430/arctic1686>
- Saucier, F. J., Senneville, S., Prinsenberg, S., Roy, F., Smith, G., Gachon, P., et al. (2004). Modelling the sea ice-ocean seasonal cycle in Hudson Bay, Foxe Basin and Hudson Strait, Canada. *Climate Dynamics*, *23*(3/4), 303–326.
- Shiklomanov, I. A., & Shiklomanov, A. I. (2003). Climatic change and the dynamics of river runoff into the Arctic Ocean. *Water Resources*, *30*(6), 593–601. <https://doi.org/10.1023/B:WARE.0000007584.73692.ca>
- Smith, G. C., Roy, F., Mann, P., Dupont, F., Brasnett, B., Lemieux, J.-F., et al. (2014). A new atmospheric dataset for forcing ice-ocean models: Evaluation of reforecasts using the Canadian global deterministic prediction system. *Quarterly Journal of the Royal Meteorological Society*, *140*(680), 881–894. <https://doi.org/10.1002/qj.2194>
- St-Laurent, P., Straneo, F., & Barber, D. G. (2012). A conceptual model of an Arctic sea. *Journal of Geophysical Research*, *117*, C06010. <https://doi.org/10.1029/2011JC007652>
- St-Laurent, P., Straneo, F., Dumais, J.-F., & Barber, D. G. (2011). What is the fate of the river waters of Hudson Bay? *Journal of Marine Systems*, *88*, 352–361.
- Steele, M., & Ermold, W. (2007). Steric sea level change in the Northern Seas. *Journal of Climate*, *20*(3), 403–417. <https://doi.org/10.1175/JCLI4022.1>
- Wang, J., Mysak, L. A., & Ingram, R. G. (1994a). Interannual variability of sea-ice cover in Hudson Bay, Baffin Bay and the Labrador Sea. *Atmosphere-Ocean*, *32*(2), 421–447. <https://doi.org/10.1080/07055900.1994.9649505>
- Wang, J., Mysak, L., & Ingram, R. (1994b). A numerical-simulation of sea-ice cover in Hudson Bay. *Journal Of Physical Oceanography*, *24*(12), 2515–2533.
- Wang, J., Mysak, L. A., & Ingram, R. G. (1994c). A three-dimensional numerical simulation of Hudson Bay summer ocean circulation: Topographic gyres, separations, and coastal jets. *Journal of Physical Oceanography*, *24*(12), 2496–2514. [https://doi.org/10.1175/1520-0485\(1994\)024h2496:ATDNSOi2.0.CO;2](https://doi.org/10.1175/1520-0485(1994)024h2496:ATDNSOi2.0.CO;2)